Ultrahigh pressure shock compression of platinum up to 1.1 TPa: Melting and ionization

Zhiguo Li,[1,*] Long Hao,[1,*] Xiang Wang,[1] Guojun Li,[1] Yong Hou,[2] Qingsong Wang,[1] Lei Liu,[3] Huayun Geng,[1] Yuying Yu,[1] Chengda Dai,[1] Qiang Wu,[1] and Jianbo Hu[1,3,†]

[1]*National Key Laboratory for Shock Wave and Detonation Physics, Institute of Fluid Physics, China Academy of Engineering Physics, Mianyang, Sichuan 621900, China*

[2]*Department of Physics, National University of Defense Technology, Changsha 410073, China*

[3]*State Key Laboratory for Environment-Friendly Energy Materials, Southwest University of Science and Technology, Mianyang 621010, China*

(Received 19 January 2024; accepted 29 March 2024; published 22 April 2024)

Shock compression experiments on platinum (Pt) were carried out by combining a two-stage gas gun with the unique high-Z three-stage gas gun launcher technique. The shock Hugoniot of Pt was determined in a wide pressure range of 0.2–1.1 TPa. These data fill the gap between the two-stage gas gun and magnetically driven shock experiments, and thereby we observe a clear softening behavior of the Pt Hugoniot at the beginning of ~1.1 TPa. *Ab initio* molecular dynamics simulations were also performed to reveal the response of Pt under ultrahigh pressure compressions. The simulation results show that the melting of Pt under shock compression occurs at ~570 GPa, and a sudden increase in conductivity and free electron number density emerges at the beginning of the Hugoniot softening. The further electronic structure calculations indicate that the Hugoniot softening may arise from the thermal excitation (ionization) of the 5d electrons and the localized 6s electrons in Pt under extreme shock compression. This work has gained further insight into the ionization behaviors of high-Z metal elements with complex electronic structures under ultrahigh pressure compressions, which is of significance for understanding the partial ionization effect in the transition region from condensed matter to warm dense matter.

DOI: 10.1103/PhysRevB.109.144109

I. INTRODUCTION

The thermodynamic properties of materials under extremely high pressure-temperature (P-T) conditions are of great significance largely due to the key applications in geophysics, planetary science, and inertial confinement fusion (ICF) [1–3]. Recent improvements in static compression and dynamic compression experimental capabilities have made it accessible to obtain terapascal (1 TPa = 1000 GPa) pressure conditions, paving the way for exploring material properties under extreme pressures [4,5]. As one of the most important standard materials in both static and dynamic high pressure experiments, platinum (Pt) has been widely used as the pressure scale for diamond anvil cell (DAC) experiments and the high-impedance reference for shock compression experiments. It is highly desirable to construct reliable pressure standards at TPa conditions for the dynamic and static extremely high pressure experiments, which strongly rely on the accurate knowledge about the equation of states (EOS) of platinum in the TPa pressure range [6,7]. A wide variety of EOS models for platinum can be found in the literature, but most of them are limited to the two-phase region of solid and liquid and pressures of a few hundred GPa. For more extreme conditions of TPa pressures and tens of thousands of kelvins (K), the bound electrons would be driven into delocalization, which makes the electronic ionization effects play an essential role in EOS models under such extreme temperature and pressure conditions. However, the effective way to treat the electronic ionization effects remains an open question. Thus the ultrahigh pressure experiments to obtain high-precision EOS data at TPa pressures are paramount in providing experimental constraints for the construction/validation of theoretical models for extreme conditions.

Platinum has been examined extensively under both static and dynamic compressions. The static compression experiments on platinum are fundamentally limited to pressures below 300 GPa and temperatures below 4000 K [8–10]. The shock compression experiments on platinum conducted through a two-stage gas gun obtained Hugoniot data not exceeding 660 GPa [11,12]. Cochrane *et al.* performed shock experiments on platinum using a Z machine at Sandia National Laboratory, obtaining the Hugoniot data in the pressure range of 1.2–2.2 TPa [13]. Fratanduono *et al.* used the National Ignition Facility (NIF) laser to generate nonshocked quasi-isentropic compression conditions and obtained the quasi-isentropic EOS data for platinum up to 1.1 TPa with little temperature rise, not exceeding 1000 K [6]. The shockless compression of Pt on the Z machine was carried out by Porwitzky *et al.*, and the principal isentrope was determined up to 650 GPa [14]. More recently, the development of *in situ* diagnosis technology for dynamic compression experiments has enabled the acquisition of the microscopic physical information during shock processes. Sharma *et al.* used *in situ* x-ray diffraction (XRD) diagnostics to achieve the measurement of platinum structure up to the shock pressure of 380 GPa in laser-driven shock experiments [15].

*These authors contributed equally to this work.
†jianbo.hu@caep.cn

Turneaure and Das implemented single-pulse (∼100 ps duration) extended x-ray absorption fine structure (EXAFS) measurements in laser-driven shock experiments on platinum, obtaining short-range structure information and determining temperature under shock pressures ranging from 72 to 325 GPa [16]. To sum up, the experimental data in the TPa pressure range is still scarce at present. Especially, there exists a gap from 0.7 to 1.2 TPa along the Hugoniot of platinum. Therefore, it is insufficient to provide effective constraints to verify and validate the theoretical models. The current wide-ranged multiphase EOS models for platinum mainly include the SESAME EOSs (No. 3740 and No. 3732) [17], the quotidian EOS (QEOS) [18], and a semiempirical EOS by Elkin *et al.* [19]. Nevertheless, these models still have discrepancies, especially under extremely high pressure conditions.

It is well known that the ionization of electrons under extremely high *P*-*T* conditions plays a critical role in constructing the theoretical model in the ionized dense plasma regime and has attracted great attention. Based on the first-principles molecular dynamics (FPMD) and path-integral Monte Carlo simulations, Hu *et al.* identified the 1*s* electron ionizations of silicon under extreme shock compression (>100 Mbar), which resulted in a second maximum compression on the Hugoniot [20]. Militzer and Driver and colleagues used a similar method to investigate the compression behavior of neon, aluminum, and magnesium under extreme shock pressures [21,22]. The *K*-shell and *L*-shell ionization of these materials were identified according to the changes of compressibility on the Hugoniot. Lazicki *et al.* performed the laser-driven planar shock experiments to compress the LiH up to 1.1 TPa, and the reflectivity measurement at the shock front revealed a metal-like reflectivity arisen from the ionization of the Li 2*s* electron [23]. The ionizations of helium and silicon under laser-driven shocks, reported by Eggert *et al.* [24] and Henderson *et al.* [25], were identified through the slope change on the measured principal Hugoniot. Kritcher *et al.* [26] and Döppner *et al.* [27] employed laser-driven capsule implosion experiments at NIF to generate spherically converging shock waves. CH and beryllium were compressed over 100 Mbar and the ionization of inner-core electrons was triggered, which was determined by x-ray Thomson scattering measurements and the increase in compressibility. All above studies have been mainly focused on the low- to medium-*Z* materials. Recently, the shock experiments on high-*Z* materials gold (Au) up to 0.9 TPa were carried out using the three-stage gas gun technique [28]. A softening behavior of the Au Hugoniot beyond ∼560 GPa was observed, which arose from the ionization of 5*d* electrons on the basis of first-principles electronic structure calculations. Overall, the electronic structures of high-*Z* elements are really complex, exerting significant influence of electron ionization on their compression behavior. Nevertheless, the research and understanding regarding this question are seriously insufficient.

In this work, hypervelocity (up to 10 km/s) shock experiments have been carried out to study the dynamic response of Pt in a wide pressure range of 0.2–1.1 TPa by combining the use of two-stage gas gun (2sGG) and a recently developed three-stage gas gun (3sGG). High-precision experimental results obtained exactly fill the gap between the data provided by previous 2sGG and magnetically driven shock experiments. A softening behavior along the shock Hugoniot of Pt was identified at an extremely high pressure of ∼1.1 TPa. The *ab initio* molecular dynamics (AIMD) calculations reveal that such softening can be attributed to the thermal excitation (ionization) of 5*d* and 6*s* electrons. The present experimental data also provide a solid constraint for discriminating between different EOS models, and they are further found to be in good agreement with the AIMD simulations and the latest SESAME model. This work gains further insight into the ionization of 5*d* metals under extreme shock conditions.

II. EXPERIMENTAL METHODS

The schematic illustration of the experimental setup is displayed in Fig. S1 of the Supplemental Material (SM) [29]. For impact velocities above 7 km/s, the shock experiments on Pt were conducted on a three-stage gas gun facility developed recently at the Institute of Fluid Physics of China Academy of Engineering Physics, in which a hypervelocity high-*Z* tantalum (Ta) flyer plate up to 10 km/s driven by the graded density impactor (GDI) impacts the target to generate TPa extreme states [30]. Figure S2 [29] shows the representative signals for the velocity history of the Ta flyer measured by a Doppler pins system (DPS) [31]. The velocity history shows that the Ta flyer experiences an initial weak shock compression and a following quasi-isentropic compression, finally reaching the terminal velocity with steadiness better than 1%. This compression path can effectively reduce the effect of shock heating on the Ta flyer. The deviation of the terminal velocities measured by each DPS is less than 0.5%. For impact velocities below 7 km/s, the shock experiments were performed through a 28 mm caliber two-stage gas gun. Shock wave front restoration technology was achieved via the utilization of 35 electrical-shorting pins (ESPs). The experimental details are provided in the SM [29]. In both 2sGG and 3sGG experiments, the shock wave transit time in the Pt sample (Δt) is determined by the difference between the shock arrival times of the ESPs at the sample rear surface and the baseplate rear surface. Figure S3 [29] shows the typical ESP measurement results of the shock arrival times in the 3sGG experiment. The shock velocity is then obtained by $U_s = d/\Delta t$, where d is the sample thickness. The shock states are deduced using the impedance matching method. The experimental uncertainties are determined by a Monte Carlo technique [32,33]. More details for the inferences of shock states, along with uncertainty analyses, can be found in our previous work [28].

III. RESULTS AND DISCUSSIONS

The obtained Pt Hugoniot data in a wide pressure range from 0.2 to 1.1 TPa are given in Table S1 of the SM [29]. Figure 1(a) shows the $U_s - U_p$ data of our experiments, along with the results obtained by previous 2sGG and the *Z* machine. It can be seen that the present 2sGG data are in good agreement with the previous 2sGG data. The Hugoniot data of 3sGG ranges from 0.7 to 1.1 TPa, filling exactly the gap between the experimental data of 2sGG and the *Z* machine. Within the region covered by 2sGG and 3sGG,

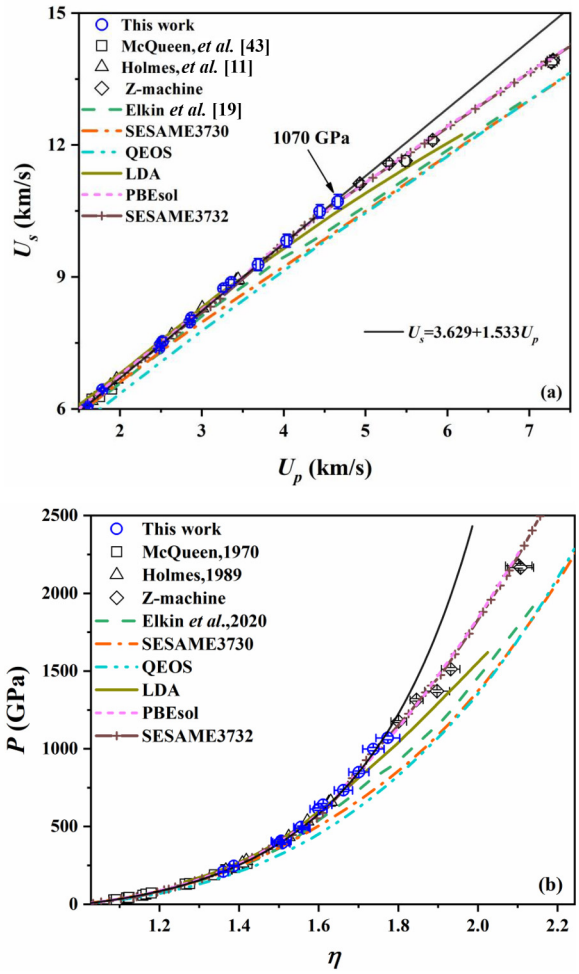

FIG. 1. Principal Hugoniot of platinum in the U_s-U_p (a) and the P-η (b) space. The open spheres are the present three-stage and two-stage gas gun data. The open squares and open up-pointing triangles are the two-stage gas gun data of McQueen *et al.* [43] and Holmes *et al.* [11], respectively. The *Z*-machine data are displayed as the open diamonds [13]. The dash, dash-dot, dash-dot-dot, and dash-plus curves are the calculations of Elkin *et al.* [19], SESAME3730 [17], QEOS [18], and SESAME3732 [17], respectively. The AIMD simulations with LDA and PBEsol [13] functionals are represented by the solid and short-dash lines, respectively. The linear $U_s - U_p$ relation obtained by fitting the present gas gun data is shown as the black solid line.

the U_s-U_p fulfills an excellent linear relationship of $U_s = 3.629 + 1.533U_p$, which is consistent with the linear relation ($U_s = 3.648 + 1.539U_p$) obtained by Holmes *et al.* [11]. Beyond the scope of 3sGG, the U_s-U_p data of the *Z* machine gradually deviate from the linear U_s-U_p relation, and exhibit a lower slope. Combining the gas gun data (including 3sGG and 2sGG data) and the *Z*-machine data, a quadratic U_s-U_p relation of $U_s = 3.511 + 1.695U_p - 0.036U_p^2$ for Pt covering a wide pressure range up to 2 TPa is obtained by using the least-squares fitting method. Figure 1(b) shows the same experimental data in the P-η space ($\eta = \rho/\rho_0$ is the compression ration). Corresponding to the bending of the U_s-U_p relation, the softening behavior of the Pt Hugoniot data begins at ∼1.1 TPa and becomes more visible with increasing shock pressures (i.e., higher compressibility compared with the Hugoniot curve derived from the linear U_s-U_p relation). The softening behavior of the shock Hugoniot was also observed in a neighbor 5*d* metal element gold (Au) recently, which occurs at ∼560 GPa shock pressure and arises from the ionization of Au 5*d* electrons under shock compressions. Obviously, the shock pressure for the occurrence of the softening of the Pt Hugoniot is much higher than that of Au, and this difference will be further analyzed in detail in the following text.

The current 3sGG data improve the experimental constraints for the EOS models of Pt by filling the gap between 2sGG and the *Z* machine. Figure 1 presents the comparison of experimental data with various theoretical models including the SESAME EOSs (No. 3730 and No. 3732), the quotidian EOS (QEOS), and the semiempirical EOS of Elkin *et al.* [19]. The calculation results of SESAME 3730 and Elkin *et al.* are consistent with 2sGG data but obviously deviate from the 3sGG and the *Z*-machine data. The calculation results of the QEOS model merge with those of SESAME 3730 and Elkin *et al.* at high shock velocities, but fail at lower shock velocities. It is worth noting that the partial ionization of electrons would occur under TPa shock conditions, and its contribution to the theoretical model has become particularly remarkable in this case. The widely used theoretical models, such as Thomas-Fermi, average atom, and INFERNO, may not be able to effectively describe this partial ionization effect and lead to the differences from the high pressure shock data. The recently developed SESAME 3732 reasonably reproduces all the gas gun and *Z*-machine data up to 2 TPa; it was constructed based on the high pressure shock data of the *Z* machine. Thus the high-precision experimental data play a fundamental role in the establishment of theoretical models.

We also performed *ab initio* molecular dynamics (AIMD) simulations using the Vienna *ab initio* simulation package (VASP) [34–36] with the local density approximation (LDA) [37] functional. The plane-wave cutoff energy of 600 eV and a 2×2×2 Monkhorst-Pack [38] k-point grid in the solid region and a Baldereschi mean-value point [39] in the liquid region were adopted. The canonical ensemble (*NVT*) and the Nosé-Hoover thermostats [40,41] were used. Details of AIMD calculations are given in the Supplemental Material [29]. The present LDA results, together with the simulation results with the Perdew-Burke-Ernzerhof functional for solids (PBEsol [42]) by Cochrane *et al.* [13] are compared with the experimental data in Fig. 1. We find that the AIMD simulation with the PBEsol functional is in excellent agreement with the Hugoniot data in a wide pressure range, indicating that the PBEsol approximation can reasonably represent the exchange-correlation interaction for Pt. The calculation of LDA coincides with the experimental data in the area below 0.8 TPa pressure but deviates from the experiments with the continuous increase of shock pressures.

The softening behavior of the shock Hugoniot is typically associated with ionic or electronic rearrangement, such as melting or electronic ionizations. To clarify the physical mechanisms driving the Hugoniot softening for Pt, AIMD simulations with the PBEsol functional were performed to examine changes in ionic and electronic properties under shock compressions. As shown by the radial distribution function (RDF) of Pt under shock conditions in Fig. 2(a), Pt has still

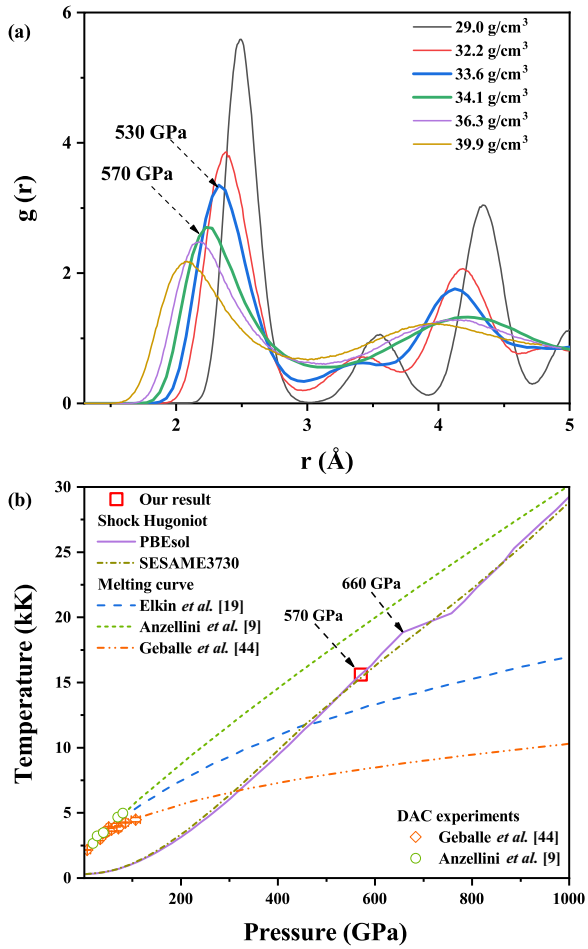

FIG. 2. (a) The radial distribution function of Pt under shock conditions; (b) the melting temperature of Pt under static and dynamic high pressures. The solid and dash-dot lines represent the shock Hugoniot calculated by the AIMD simulations with PBEsol functional [13] and SESAME3730 EOS [17], respectively. The short dash and dash-dot-dot lines are the melting curve by fitting the DAC experimental data of Anzellini *et al.* [9] and Geballe *et al.* [44], respectively. The long dash lines are the melting curve from the semiempirical EOS of Elkin *et al.* [19]. The open square is the melting temperature of Pt under shock compressions based on our RDF calculations.

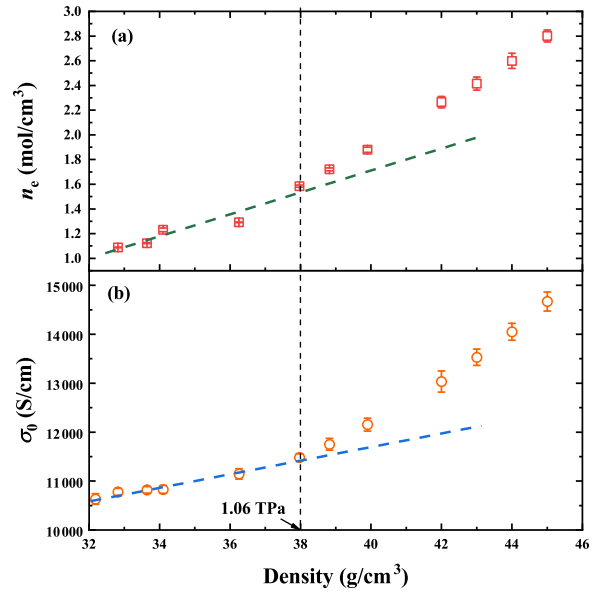

FIG. 3. *Ab initio* calculations for the free electron number density n_e (a) and dc conductivity σ_0 (b) at shock conditions of Pt. The superlinear behavior for both n_e and σ_0 appears when the shock pressure exceeds ~1.06 TPa.

shown the long-range order characteristics for pressure below 530 GPa. When the shock pressure exceeds 570 GPa, Pt has lost the long-range order features, which suggests the melting of Pt. It is worth mentioning that there is still no consensus on the melting of platinum under high pressures. In Fig. 2(b), we summarize the melting temperatures of Pt under static and dynamic high pressure conditions. The melting temperature of Pt under shock compressions is 15.6 kK at 570 GPa based on our RDF calculations. The shock Hugoniot calculated by AIMD simulations with the PBEsol functional shows a slope change at the beginning of 660 GPa (the corresponding temperature is 18.8 kK), which is a remarkable signature of melting. Nevertheless, the shock Hugoniot by SESAME3730 does not have the feature of slope change. The melting curve of Pt was also investigated by the static high pressure experiments, but the maximum pressure has been limited below 200 GPa currently. Therefore, Simon's fitting method was generally used to extrapolate the results to high pressure conditions. The melting curve determined by Anzellini *et al.* [9] significantly overestimated the melting temperature, because Pt has not melted even under 1000 GPa shock conditions based on their results. The melting curve determined by Geballe *et al.* [44] significantly underestimated the melting temperature, because the laser shock experiments on Pt with *in situ* x-ray diffraction measurements have shown that Pt retained the face-centered cubic (fcc) structure to over 380 GPa. The melting curve from the semiempirical EOS of Elkin *et al.* is more reasonable than those of Anzellini *et al.* and Geballe *et al.*, but still deviates from our RDF results and the AIMD calculations of Cochrane *et al.* [13]. Overall, the controversy regarding the high pressure melting of Pt is unfavorable for elucidating the Hugoniot softening, and the sound velocity and *in situ* XRD measurements under higher shock pressure conditions are highly desirable to clarify this issue.

The electronic ionization effect is a major factor contributing to Hugoniot softening under extreme shock compressions. For a more direct and quantitative characterization of the electronic ionization effect, we further calculated the electronic conductivity through the Kubo-Greenwood formula [45,46] and derived the free electron number density n_e by fitting the real part of the frequency-dependent electrical conductivity with a Smith-Drude model [47]. Figure 3 shows the derived n_e and dc conductivity σ_0 of Pt under the shock conditions. Both n_e and σ_0 present a superlinear trend along with the increasing shock compressions with an inflection at ~38 g/cm^3 (the corresponding shock pressure is ~1.06 TPa), which coincides with the onset of the softening in the Hugoniot. Beyond the inflection point, the rapid increase of free electrons strongly suggests the ionization of some bound electrons, thereby increasing the conductivity. These results illustrate that the

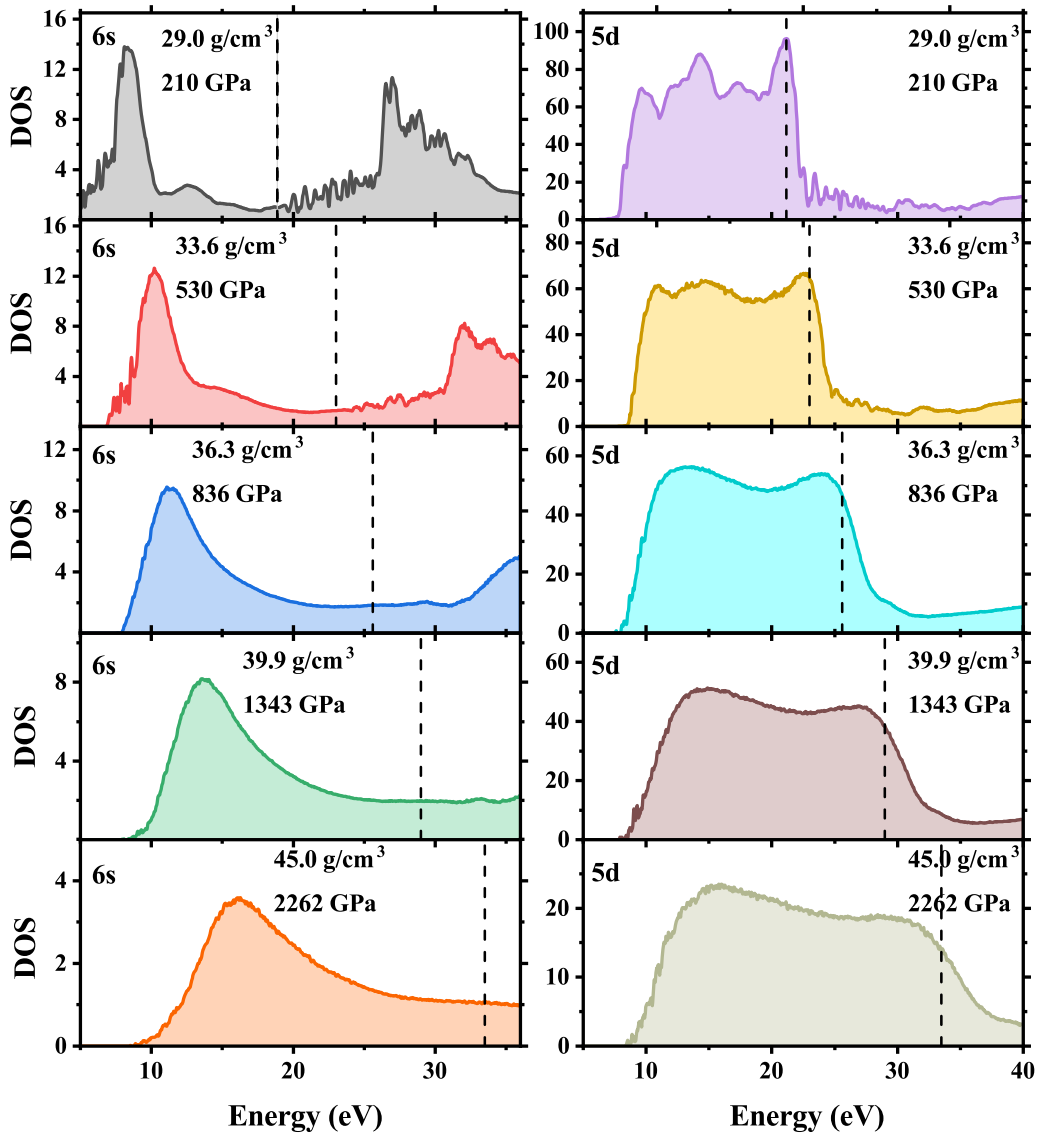

FIG. 4. *Ab initio* calculations of the DOSs of the 6*s* band (left panel) and 5*d* band (right panel) for the shocked Pt. The black dash lines represent the Fermi level.

Hugoniot softening of platinum mostly arises from the ionization effect of electrons under extreme shock compressions.

In our previous work for another 5*d* metal, Au, which is closely adjacent to Pt, the Hugoniot softening was quantitatively identified as the result of ionizations of 5*d* electrons through the analysis of the electronic structure of Au via *ab initio* calculations [28], but it should be noted that the shock pressure (∼560 GPa) for the occurrence of Au Hugoniot softening is much smaller than that for Pt (∼1070 GPa). Here, the electronic structure of Pt under shock conditions was calculated and a comparative analysis with Au was performed to investigate the physical law and mechanism that drives the ionization of 5*d* metal under extreme shock compressions. The calculated densities of state (DOSs) for the shocked Pt are presented in Fig. 4. Similar to Au, the 5*d* band of Pt (right panel) also exhibits relatively strong localized behavior for low shock compressions, but there is a remarkable difference: the 5*d* band of Pt crosses the Fermi level, whereas the 5*d* band of Au lies below the Fermi level and an obvious energy gap exists from the top of the 5*d* band to the Fermi level. With increasing shock pressures and temperatures, the 5*d* electronic band of Pt broadens and shifts upward. Thus, the thermal excitation of Pt 5*d* electrons will continue to occur as the shock density and temperature increase, due to the fact that the 5*d* band crosses the Fermi level and there is not an energy gap to overcome like that of Au. As for the 6*s* band of Pt (left panel), a highly localized state below the Fermi level can be clearly observed at 29 g/cm^3. Also, this localized state exhibits broadening and an upward shift with increasing shock density and temperature. Therefore, the 6*s* electrons in this localized state will undergo ionization as the shock temperature and density increase. Based on the above analysis, we may draw the conclusion that the ionization of Pt 5*d* electrons under shock compression would gradually occur with the increase of shock pressure and temperature. At the onset of the Hugoniot softening (the density is ∼38.0 g/cm^3 and the temperature is ∼31 000 K), the ionization of 6*s* electrons in the localized state was triggered and driven by

both pressure and temperature effects, i.e., the pressure broadens and raises the localized 6*s* band, while the temperature provides the energy needed for the electrons to transit above the Fermi level. The superlinear trend of conductivity and the softening manner of the Hugoniot arise exactly from the ionization of localized electrons, which contribute substantial free (ionization) electrons and partially consume the system energy that should increase the shock pressure.

IV. CONCLUSIONS

In summary, high-precision shock data for platinum in a wide pressure range from 0.2 to 1.1 TPa have been obtained by combining the high-*Z* three-stage gas gun and two-stage gas gun shock experiments. These data fill the gap between the previous two-stage gas gun and magnetically driven shock experiments and provide important constraints for various theoretical models in the transition region from the condensed matter to the WDM. It is found that the recently developed SESAME3732 models and the AIMD simulations with PBEsol functional can well reproduce the experimental data. We observe a softening behavior of the Pt Hugoniot for pressure beyond ∼1.1 TPa. The *ab initio* molecular dynamics simulation results show a sudden increase of conductivity and free electron number density emerging at the beginning of the Hugoniot softening. Further electronic structure calculations indicate that the Hugoniot softening may arise from the thermal excitation (ionization) of the 5*d* electrons and the localized 6*s* electrons in Pt under extreme shock compressions. The present work is of importance to build a high-precision pressure standard up to TPa pressures and provide a fundamental input for modeling the transition region from condensed matter to warm dense matter, which exerts a far-reaching impact in the fields of high pressure science, ICF, astrophysics, and planetary physics.

ACKNOWLEDGMENT

We thank our colleagues for the gas-gun operation. This work was supported by the National Natural Science Foundation of China (Grants No. 12072331, No. 12174357, and No. 12204387).

[1] P. Wang, C. Zhang, S. Jiang, X. Duan, H. Zhang, L. Li, W. Yang, Y. Liu, Y. Li, L. Sun, H. Liu, and Z. Wang, Density-dependent shock Hugoniot of polycrystalline diamond at pressures relevant to ICF, Matter Radiat. Extremes **6**, 035902 (2021).

[2] S. X. Hu, D. T. Bishel, D. A. Chin, P. M. Nilson, V. V. Karasiev, I. E. Golovkin, M. Gu, S. B. Hansen, D. I. Mihaylov, N. R. Shaffer, S. Zhang, and T. Walton, Probing atomic physics at ultrahigh pressure using laser-driven implosions, Nat. Commun. **13**, 6780 (2022).

[3] R. G. Kraus, S. Root, R. W. Lemke, S. T. Stewart, S. B. Jacobsen, and T. R. Mattsson, Impact vaporization of planetesimal cores in the late stages of planet formation, Nat. Geosci. **8**, 269 (2015).

[4] P. Kalita, K. R. Cochrane, M. D. Knudson, T. Ao, C. Blada, J. Jackson, J. Gluth, H. Hanshaw, E. Scoglietti, and S. D. Crockett, Ti-6Al-4V to over 1.2 TPa: Shock Hugoniot experiments, *ab initio* calculations, and a broad-range multiphase equation of state, Phys. Rev. B **107**, 094101 (2023).

[5] A. Dewaele, P. Loubeyre, F. Occelli, O. Marie, and M. Mezouar, Toroidal diamond anvil cell for detailed measurements under extreme static pressures, Nat. Commun. **9**, 2913 (2018).

[6] D. E. Fratanduono, M. Millot, D. G. Braun, S. J. Ali, A. Fernandez-Pañella, C. T. Seagle, J. P. Davis, J. L. Brown, Y. Akahama, R. G. Kraus, M. C. Marshall, R. F. Smith, E. F. O'Bannon, J. M. McNaney, and J. H. Eggert, Establishing gold and platinum standards to 1 terapascal using shockless compression, Science **372**, 1063 (2021).

[7] L. Burakovsky, D. L. Preston, S. D. Ramsey, C. E. Starrett, and R. S. Baty, Shock standards Cu, Ag, Ir, and Pt in a wide pressure range, Matter Radiat. Extremes **8**, 046901 (2023).

[8] C.-S. Zha, K. Mibe, W. A. Bassett, O. T. schauner, H.-K. Mao, and R. J. Hemley, *P-V-T* equation of state of platinum to 80 GPa and 1900 K from internal resistive heating/x-ray diffraction measurements, J. Appl. Phys. **103**, 054908 (2008).

[9] S. Anzellini, V. Monteseguro, E. Bandiello, A. Dewaele, L. Burakovsky, and D. Errandonea, *In situ* characterization of the high pressure–high temperature melting curve of platinum, Sci. Rep. **9**, 13034 (2019).

[10] A. Dewaele, P. Loubeyre, and M. Mezouar, Equations of state of six metals above 94 GPa, Phys. Rev. B **70**, 094112 (2004).

[11] N. C. Holmes, J. A. Moriarty, G. R. Gathers, and W. J. Nellis, The equation of state of platinum to 660 GPa (6.6 Mbar), J. Appl. Phys. **66**, 2962 (1989).

[12] *LASL Shock Hugoniot Data*, edited by S. P. Marsh, Los Alamos Series on Dynamic Material Properties (University of California Press, Berkeley, CA, 1980).

[13] K. R. Cochrane, P. Kalita, J. L. Brown, C. A. McCoy, J. W. Gluth, H. L. Hanshaw, E. Scoglietti, M. D. Knudson, S. P. Rudin, and S. D. Crockett, Platinum equation of state to greater than two terapascals: Experimental data and analytical models, Phys. Rev. B **105**, 224109 (2022).

[14] A. Porwitzky, J. Brown, S. Duwal, D. H. Dolan, C. Blada, J. Boerner, J. Williams, and S. Payne, Reduced scale stripline platform to extend accessible pressures on the *Z* machine: Shockless compression of platinum to 650 GPa, J. Appl. Phys. **132**, 115102 (2022).

[15] S. M. Sharma, S. J. Turneaure, J. M. Winey, and Y. M. Gupta, What determines the fcc-bcc structural transformation in shock compressed noble metals?, Phys. Rev. Lett. **124**, 235701 (2020).

[16] S. J. Turneaure and P. Das, Vibrational response and temperature of shock-compressed Pt: *In situ* extended x-ray absorption fine structure measurements to 325 GPa, Phys. Rev. B **105**, 174103 (2022).

[17] S. P. Lyon and J. D. Johnson, SESAME: The Los Alamos National Laboratory Equation of State Database, Report No. LA-UR-92-34071992.

[18] S. Faik, A. Tauschwitz, and I. Iosilevskiy, The equation of state package FEOS for high energy density matter, Comput. Phys. Commun. **227**, 117 (2018).

[19] V. M. Elkin, V. N. Mikhaylov, A. A. Ovechkin, and N. A. Smirnov, A wide-range multiphase equation of state for platinum, J. Phys.: Condens. Matter **32**, 435403 (2020).

[20] S. X. Hu, B. Militzer, L. A. Collins, K. P. Driver, and J. D. Kress, First-principles prediction of the softening of the silicon shock Hugoniot curve, Phys. Rev. B **94**, 094109 (2016).

[21] K. P. Driver, F. Soubiran, and B. Militzer, Path integral Monte Carlo simulations of warm dense aluminum, Phys. Rev. E **97**, 063207 (2018).

[22] B. Militzer, F. Gonzalez-Cataldo, S. Zhang, K. P. Driver, and F. Soubiran, First-principles equation of state database for warm dense matter computation, Phys. Rev. E **103**, 013203 (2021).

[23] A. Lazicki, R. A. London, F. Coppari, D. Erskine, H. D. Whitley, K. J. Caspersen, D. E. Fratanduono, M. A. Morales, P. M. Celliers, J. H. Eggert, M. Millot, D. C. Swift, G. W. Collins, S. O. Kucheyev, J. I. Castor, and J. Nilsen, Shock equation of state of ^{6}LiH to 1.1 TPa, Phys. Rev. B **96**, 134101 (2017).

[24] J. Eggert, S. Brygoo, P. Loubeyre, R. S. McWilliams, P. M. Celliers, D. G. Hicks, T. R. Boehly, R. Jeanloz, and G. W. Collins, Hugoniot data for helium in the ionization regime, Phys. Rev. Lett. **100**, 124503 (2008).

[25] B. J. Henderson, M. C. Marshall, T. R. Boehly, R. Paul, C. A. McCoy, S. X. Hu, D. N. Polsin, L. E. Crandall, M. F. Huff, D. A. Chin, J. J. Ruby, X. Gong, D. E. Fratanduono, J. H. Eggert, J. R. Rygg, and G. W. Collins, Shock-compressed silicon: Hugoniot and sound speed up to 2100 GPa, Phys. Rev. B **103**, 094115 (2021).

[26] A. L. Kritcher, D. C. Swift, T. Doppner, B. Bachmann, L. X. Benedict, G. W. Collins, J. L. DuBois, F. Elsner, G. Fontaine, J. A. Gaffney, S. Hamel, A. Lazicki, W. R. Johnson, N. Kostinski, D. Kraus, M. J. MacDonald, B. Maddox, M. E. Martin, P. Neumayer, A. Nikroo *et al.*, A measurement of the equation of state of carbon envelopes of white dwarfs, Nature **584**, 51 (2020).

[27] T. Döppner, M. Bethkenhagen, D. Kraus, P. Neumayer, D. A. Chapman, B. Bachmann, R. A. Baggott, M. P. Bohme, L. Divol, R. W. Falcone, L. B. Fletcher, O. L. Landen, M. J. MacDonald, A. M. Saunders, M. Schorner, P. A. Sterne, J. Vorberger, B. B. L. Witte, A. Yi, R. Redmer *et al.*, Observing the onset of pressure-driven *K*-shell delocalization, Nature **618**, 270 (2023).

[28] Z. Li, X. Wang, Y. Hou, Y. Yu, G. Li, L. Hao, X. Li, H. Geng, C. Dai, Q. Wu, H. K. Mao, and J. Hu, Quantifying the partial ionization effect of gold in the transition region between condensed matter and warm dense matter, Proc. Natl. Acad. Sci. USA **120**, e2300066120 (2023).

[29] See Supplemental Material at http://link.aps.org/supplemental/10.1103/PhysRevB.109.144109 for summaries of the experimental and theoretical methods, and Figs. S1–S3 and Tables S1, which include Refs. [34–42,45–47]

[30] X. Wang, C. Dai, Q. Wang, L. Hao, J. Bai, Y. Yu, Q. Wu, H. Tan, J. Hu, G. Luo, Q. Shen, and L. Zhang, Development of a three-stage gas gun launcher for ultrahigh-pressure Hugoniot measurements, Rev. Sci. Instrum. **90**, 013903 (2019).

[31] J. Weng, X. Wang, Y. Ma, H. Tan, L. Cai, J. Li, and C. Liu, A compact all-fiber displacement interferometer for measuring the foil velocity driven by laser, Rev. Sci. Instrum. **79**, 113101 (2008).

[32] Z.-G. Li, Q.-F. Chen, Y.-J. Gu, J. Zheng, W. Zhang, L. Liu, G.-J. Li, Z.-Q. Wang, and J.-Y. Dai, Multishock compression of dense cryogenic hydrogen-helium mixtures up to 60 GPa: Validating the equation of state calculated from first principles, Phys. Rev. B **98**, 064101 (2018).

[33] G.-J. Li, Z.-G. Li, Q.-F. Chen, Y.-J. Gu, W. Zhang, L. Liu, H.-Y. Geng, Z.-Q. Wang, Y.-S. Lan, Y. Hou, J.-Y. Dai, and X.-R. Chen, Multishock to quasi-isentropic compression of dense gaseous deuterium-helium mixtures up to 120 GPa: Probing the sound velocities relevant to planetary interiors, Phys. Rev. Lett. **126**, 075701 (2021).

[34] G. Kresse and J. Furthmüller, Efficient iterative schemes for *ab initio* total-energy calculations using a plane-wave basis set, Phys. Rev. B **54**, 11169 (1996).

[35] G. Kresse and D. Joubert, From ultrasoft pseudopotentials to the projector augmented-wave method, Phys. Rev. B **59**, 1758 (1999).

[36] P. E. Blöchl, Projector augmented-wave method, Phys. Rev. B **50**, 17953 (1994).

[37] J. P. Perdew and Y. Wang, Accurate and simple analytic representation of the electron-gas correlation energy, Phys. Rev. B **45**, 13244 (1992).

[38] H. J. Monkhorst and J. D. Pack, Special points for Brillouin-zone integrations, Phys. Rev. B **13**, 5188 (1976).

[39] A. Baldereschi, Mean-value point in the Brillouin zone, Phys. Rev. B **7**, 5212 (1973).

[40] W. G. Hoover, Canonical dynamics: Equilibrium phase-space distributions, Phys. Rev. A **31**, 1695 (1985).

[41] S. Nosé, A unified formulation of the constant temperature molecular dynamics methods, J. Chem. Phys. **81**, 511 (1984).

[42] J. P. Perdew, A. Ruzsinszky, G. I. Csonka, O. A. Vydrov, G. E. Scuseria, L. A. Constantin, X. Zhou, and K. Burke, Restoring the density-gradient expansion for exchange in solids and surfaces, Phys. Rev. Lett., **100**, 136406 (2008).

[43] R. G. McQueen, S. P. Marsh, J. W. Taylor, J. M. Fritz, and W. J. Carter, in *High Velocity Impact Phenomena*, edited by R. Kinslow (Academic Press, New York, 1970), Chap. VII.

[44] Z. M. Geballe, N. Holtgrewe, A. Karandikar, E. Greenberg, V. B. Prakapenka, and A. F. Goncharov, Latent heat method to detect melting and freezing of metals at megabar pressures, Phys. Rev. Mater. **5**, 033803 (2021).

[45] R. Kubo, Statistical-mechanical theory of irreversible processes. I. General theory and simple applications to magnetic and conduction problems, J. Phys. Soc. Jpn. **12**, 570 (1957).

[46] D. A. Greenwood, The Boltzmann equation in the theory of electrical conduction in metals, Proc. Phys. Soc. **71**, 585 (1958).

[47] N. Smith, Classical generalization of the Drude formula for the optical conductivity, Phys. Rev. B **64**, 155106 (2001).